Journal of Alloys and Compounds 699 (2017) 126–135

Contents lists available at ScienceDirect

Journal of Alloys and Compounds

journal homepage: http://www.elsevier.com/locate/jalcom

Self-supported binder-free carbon fibers/MnO_2 electrodes derived from disposable bamboo chopsticks for high-performance supercapacitors

Yuxiang Wen [a], Tianfeng Qin [a], Zilei Wang [a], Xinyu Jiang [a], Shanglong Peng [a, b, *], Jiachi Zhang [a], Juan Hou [c], Fei Huang [b], Deyan He [a], Guozhong Cao [b, **]

[a] School of Physical Science and Technology, Key Laboratory for Magnetism and Magnetic Materials of the Ministry of Education, Lanzhou University, Lanzhou, 730000, China
[b] Department of Materials Science and Engineering, University of Washington, Seattle, WA, 98195-2120, United States
[c] School of Science, Key Laboratory of Ecophysics and Department of Physics, Shihezi University, Xinjiang, 832003, China

ARTICLE INFO

Article history:
Received 20 October 2016
Received in revised form
17 December 2016
Accepted 26 December 2016
Available online 27 December 2016

Keywords:
Disposable bamboo chopsticks
Carbon fibers
Manganese dioxide
Self-supported
Supercapacitors

ABSTRACT

The increasing market growth of hybrid vehicles requires not only improvement on supercapacitor performance, but also cheap, abundant and sustainable material for supercapacitor fabrication. The present study demonstrated a novel strategy to convert used disposable bamboo chopsticks into uniform carbon fibers, and subsequently manganese dioxide (MnO_2) was conformably grown on each fiber to form a carbon fiber/MnO_2 composite. When it used as a self-supported binder-free electrode for supercapacitors, it delivered a superior mechanical stability, excellent rate capability, high specific capacitance of 375 F g^{-1} at the current density of 1 A g^{-1} and an increase specific capacitance was found after 5000 cycles interestingly. Moreover, the symmetric supercapacitor comprised of CFS/MnO_2 electrodes presents a maximum energy density of 11 Wh kg^{-1} and a maximum power density of 17.4 kW kg^{-1}. In addition, this approach presents a scalable, low-cost and sustainable route to transform chopsticks waste into carbon fibers to make electrodes for supercapacitors and lithium-ion capacitors.

1. Introduction

The ever-increasing market penetration of hybrid or all-electric vehicles requires not only a continual improvement of the performance for energy storage devices (particularly on fast charge output/storage) but also the cost minimization of the devices as much as possible [1,2]. Among the various energy storage devices, supercapacitors have been extensively recognized and are considered as an innovative energy storage systems due to higher power densities (compared with batteries) and larger energy densities (compared with conventional dielectric capacitors) [3–5]. Up to now, various active materials consisting of the carbon-based materials, metal oxides and conducting polymers have been widely used as electrodes for supercapacitors [6,7]. Among various electrode materials for supercapacitors, manganese dioxide (MnO_2) has been widely thought to be one of the most promising materials as supercapacitor electrodes because of its low cost, abundant resource and environmentally friendly [8]. MnO_2 also possesses great electrochemical properties, such as fast charge-discharge process, chemical stability, wide electrochemical potential window and a high theoretical specific capacity through Faradaic reactions (1370 F/g) [9]. However, MnO_2 has low electrical conductivity (10^{-5}–10^{-6} S/cm) that results in a serious capacitance loss particularly at a large current density, thus limiting its wide energy storage applications [10]. Carbon materials, particularly with high degrees of graphitization, possess excellent electrical conductivity, but are limited with low capacity [11–13]. Recently, there have been increasing attempts to design and synthesize novel hybrid electrodes via the coupling of various materials for supercapacitors through synergistic combination of electrical and electrochemical properties of individual electroactive materials while minimizing the impacts of the inherent limitations of individual constituent materials [14–16].

* Corresponding author. School of Physical Science and Technology, Key Laboratory for Magnetism and Magnetic Materials of the Ministry of Education, Lanzhou University, Lanzhou, 730000, China.
** Corresponding author.
E-mail addresses: pengshl@lzu.edu.cn (S. Peng), gzcao@u.washington.edu (G. Cao).

http://dx.doi.org/10.1016/j.jallcom.2016.12.330
0925-8388/

Most hybrid electrodes studied so far required metal backing foils and binders to ensure good electrical contacts between electrode materials and substrates [17–19]. However, these features added extra inert mass to the devices, which introduces undesirable mass and volume, and reduces both energy and power densities (gravimetrically and volumetrically). Binder-free and self-supported electrodes have attracted increasing attention due to their high specific capacity, excellent rate capability, and large charging/discharging potential window, which is another key component of supercapacitors [20–22]. Binder-free and self-supported carbon/MnO_2 electrodes are promising to improving the electrochemical performance of supercapacitors by eliminating both insulating polymer binder and conductive agent commonly used to enhance the electrical conductivity and mechanical integrity of the electrodes. Fang et al. have developed a type of self-supported supercapacitor electrodes with remarkably high specific capacitance by homogeneously coating polypyrrole (PPy) on multi-walled carbon nanotube membranes [23]. More recently, Qin et al. have designed and fabricated a freestanding flexible grapheme foams@PPy@MnO_2 electrode with high performance under the assistance of PPy [24].

On the other hand, sustainable low-cost natural resources are in favor for the large-scale production of electrode material. Bamboo has been studied as raw material to fabricate carbon fiber by virtue of its unique fibrous structure [25,26]. Disposable bamboo chopsticks can be converted into excellent carbon fibers sheet via simple alkaline corrosion and pyrolysis process [1]. Compared with other carbon-based materials, carbon fibers sheets derived from disposable bamboo chopsticks showed great promises including abundant-source, low-cost, facile, environmental benign and high yield [27,28]. However, the energy density of carbon fibers is yet problematic to meet the ever-growing demand for high energy-storage applications. Researchers have studied various strategies to modify the surface chemistry of carbon fibers, either by growth of functional metal oxides on fiber scaffold or doping active elements (like B, N, F and P etc.) into the fibrous carbon host, with appreciable advancement in energy storage properties [3,29,30].

The present investigation combines the merits of the high conductivity of carbon material with the ultrahigh capacity of MnO_2. Disposable bamboo chopsticks were first utilized as raw material to prepare self-supported carbon fiber substrate by means of alkaline etching and pyrolysis. Then MnO_2 was deposited directly on the as-prepared carbon fibers sheet via utilizing a simple constant current electrodeposition method. The resultant nanostructured hybrid electrodes for supercapacitors delivered a high specific capacity of 375 F g^{-1} at the current density of 1 A g^{-1}, superior cyclic performance and excellent rate capability. This work may also provide an effective solution to circumvent the environmental impact and enormous waste of forest resources caused by the use of chopsticks and develop the possible high-performance electrodes for supercapacitors.

2. Experimental procedure

All the reagents used in the experiment are of analytical grade without further purification.

2.1. Fabrication of carbon fibers sheet (CFS) substrate

The fabrication process of the carbon fibers sheet is shown in Fig. 1. The disposable bamboo chopsticks were utilized as carbon source and recycled from the canteens of Lanzhou University. The cleaned chopsticks were processed initially into debris (length: ~1 cm, width: ~0.3 cm; thickness: ~0.5 mm) using a penknife bought from local stationer before alkaline corrosion. During the following hydrothermal treatment, 1 g of processed bamboo debris were added into 100 mL of Teflon-lined stainless steel autoclave wherein a 70 mL of homogeneous 3 M KOH solution was contained. Then, the autoclave was sealed and still in an electric oven at 150 °C for 6 h. When cooled down to room temperature naturally, the samples were fetched out, and filtered by vacuum filtration with membrane filter paper into thin circular sheet (diameter: ~2.8 cm, thickness: ~1 mm), washed by ultrasonication in 100 mL distilled water for 15 min and dried at 60 °C in an electric oven overnight. Next, the circular thin sheet product was calcined at 800 °C for 2 h under the protection of Ar flow. Finally, the evolved self-supported carbon fibers sheet (diameter: ~2.5 cm, thickness: ~0.5 mm) was rinsed with 0.1 M HCl to remove the residual KOH and dried at 60 °C overnight.

2.2. Preparation of carbon fibers sheet/MnO_2 (CFS/MnO_2) electrode

Free-standing hybrid electrode material of nanostructured CFS/MnO_2 was synthesized by directly electrodepositing MnO_2 onto the CFS. In details, the CFS/MnO_2 electrode was prepared as follows: the electrolyte was consisted of 0.66 M $MnSO_4$ containing 0.34 M H_2SO_4. The self-supported carbon fibers sheet prepared in the present work was used as the working electrode for the electrodeposition of MnO_2, a self-made copper foil (length: ~1 cm, width: ~1 cm; thickness: ~0.5 mm) and a saturated calomel electrode were used as the counter electrode and reference electrode, respectively. To avoid the concentration polarization during the electrodeposition as much as possible, the anode materials of CFS must be immersed in 0.66 M $MnSO_4$ containing 0.34 M H_2SO_4 at 85 °C for 2 h before electrodeposition. Then, the MnO_2 was electrodeposited galvanostatically onto the semi-circular carbon fibers sheet at a current density of 0.05 mA cm^{-2} for 6.5 h. The obtained CFS/MnO_2 hybrid electrodes were rinsed with distilled water and 1 M KOH aqueous solution for neutralization for several times and dried in an electric oven at 60 °C overnight. The mass of MnO_2 was calculated from the difference of carbon fibers sheet and prepared CFS/MnO_2 by weighing them before and after electrodeposition.

2.3. Material characterization

The microstructure and morphology were investigated by using field emission scanning electron microscope (FE-SEM, Hitachi S-4800) and transmission electron microscopy (TEM, FEI Tecnai G2 F30 microscope operated at 300 KV). XRD measurements were performed on a Rigaku D/MAX-2400 X-ray diffractometer using Cu Kα radiation (λ = 0.154056 nm). The chemical component was analyzed on a micro-Raman spectroscope (JY-HR800, 532-nm wavelength YAG laser) and a multifunctional X-ray photoelectron spectroscope (PHI-5702, Mg KR X-ray, 1253.6 eV).

2.4. Electrochemical measurements

All electrochemical performance measurements were carried out at room temperature using an electrochemical workstation (CHI660E, CH Instrument In, Shanghai). The used conventional three electrode cell and 1 M Na_2SO_4 served as electrolyte at room temperature. The used three-electrode cell system consisted of CFS/MnO_2 as the working electrode directly, Pt plate as a counter electrode and saturated calomel electrode as the reference electrode. A potential window from 0 to 1 V was selected in all measurements. Cyclic voltammogram (CV) were performed at various scan rates ranging from 5 to 100 mV s^{-1}. Galvanostatic charge/discharge (GCD) testing were conducted at current densities from 1 to 50 A g^{-1}. Electrochemical impedance spectroscopy (EIS) were measured over a frequency range from 10^5 to 0.01 Hz at open circuit

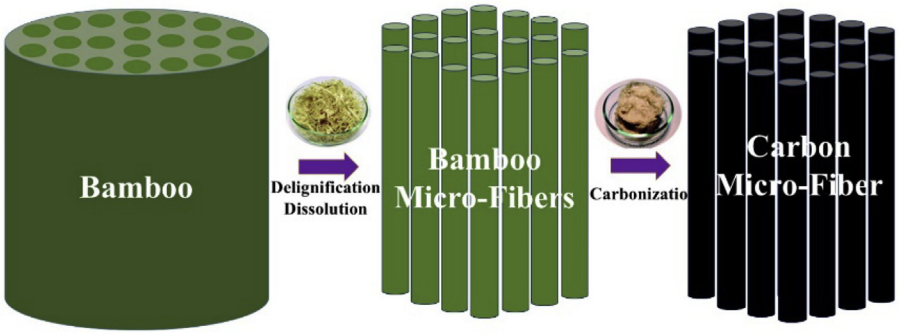

Fig. 1. The fabrication process of the carbon fibers sheet.

potential with alternating current voltage amplitude of 5 mV. The specific capacitance, C_m (F g^{-1}), was calculated from the discharge curve based on the following formula (1):

$$C_m = \frac{I\nabla t}{mV} \tag{1}$$

where I, ∇t, V and m are discharging current (A), discharging time (s), voltage change (V) and mass of electroactive material (g), respectively.

As for the best practice method for determining an electrode materials performance for supercapacitors, the two-electrode system should be used for testing process to compare it with three-electrode system [31]. The symmetric supercapacitor of CFS/MnO_2//CFS/MnO_2 was measured in a two-electrode system in which the shapes and sizes of electrodes were the same as the single electrode. The specific capacitance of the supercapacitors derived from the GCD testing through the two-electrode system was determined according to the formula (1), where m is the MnO_2 mass of the two electrodes. The energy density, E (Wh Kg^{-1}) and the power density, P (W kg^{-1}) were calculated from GCD testing according to the following formulas (2), (3), respectively:

$$E = \frac{C_m V^2}{7.2} \tag{2}$$

$$P = \frac{3600E}{\nabla t} \tag{3}$$

where C_m, V and ∇t are the specific capacitance (F g^{-1}), voltage change (V) and discharge time (s), respectively.

3. Results and discussion

Fig. 1 shows the photographs of the CFS samples evolved from bamboo chopsticks in the process of preparation. It is obvious to observe that the CFS sample has the characteristics of self-supported binder-free, can be directly used as electrode. The structure and morphology of the composites were characterized by SEM and TEM. Fig. 2(a) shows the morphology and structure of CFS evolved from bamboo chopsticks, with fibrous products dispersed and interconnected. Thin wrinkles were observed on the surface of carbon fibers and it was further confirmed by the TEM image as shown in Fig. 2(c). Such surface defects may be beneficial to the deposition and adhesion of other functional active materials [32]. The inset in Fig. 2(c) is a typical selected-area electron diffraction (SAED) pattern taken on a carbon fiber, which shows an amorphous structure of the carbon fiber [33]. The first two diffraction rings of the SAED pattern are in good accordance with (002) and (101) lattice planes of graphitic carbon [34,35]. As shown in Fig. 2(d), the carbon fiber is hollow and tubular with the inner diameter of approximately 500 nm. Carbon fibers were corroded and activated by alkaline solution (KOH) under the high temperature of 150 °C by the following reaction (4) [36]:

$$6KOH + 2C \rightarrow 2K + 3H_2 + 2K_2CO_3 \tag{4}$$

Fig. 3 presents the SEM and TEM images of the CFS/MnO_2 composites. MnO_2 was electrodeposited uniformly on the surface of CFS as shown in Fig. 3(a) and (c). Fig. 3(b) shows that MnO_2 coated on the surface of CFS is mainly nanoparticles. And the enlarged view of the TEM image also evidences that MnO_2 consists of nanoparticles with the diameter of 20–50 nm in Fig. 3(d). The electrochemical deposition of MnO_2 on carbon fibers substrate in the work electrode occurs via the following multistep reactions [37]:

$$Mn^{2+}_{bulk} \rightarrow Mn^{2+}_{surface} \tag{5}$$

$$Mn^{2+}_{surface} \rightarrow Mn^{3+}_{ads} + e^- \tag{6}$$

$$H_2O \rightarrow OH_{ads} + H^+ + e^- \tag{7}$$

$$2Mn^{3+}_{ads} \rightarrow Mn^{2+}_{ads} + Mn^{4+}_{ads} \tag{8}$$

$$Mn^{2+}_{ads} + 2OH_{ads} \rightarrow MnO_2 + 2H^+ \tag{9}$$

$$Mn^{4+}_{ads} + 2H_2O \rightarrow MnO_2 + 4H^+ \tag{10}$$

Mn^{2+} ions in electrolyte diffuse to CFS surface and was oxidized to Mn^{3+} with simultaneous oxidation of H_2O molecules producing adsorbed OH radicals. Then, Mn^{3+} ions dissociated into Mn^{2+} and Mn^{4+} ions in the adsorbed state due to these Mn^{3+} ions are unstable. Finally, MnO_2 is formed on the surface of CFS. Such a complex process leading to the formation of MnO_2 from Mn^{2+} ions can be roughly regarded as the following overall reactions of anode and cathode (11, 12):

$$\text{Anode}: \quad Mn^{2+} + 2H_2O \rightarrow MnO_2 + 4H^+ + 2e^- \tag{11}$$

$$\text{Cathode}: \quad 2H^+ + 2e^- \rightarrow H_2 \tag{12}$$

It is obvious that the kinetics of the reaction is influenced by the concentrations of Mn^{2+} ions and H^+ ions. Therefore, the electrolyte was consisted of 0.66 M $MnSO_4$ containing 0.34 M H_2SO_4. In present wok, the pH value is ~0.17 according to the formula of $pH = -\lg(C_{H^+})$ and C_{H^+} is the concentration of hydrogen ions. In the

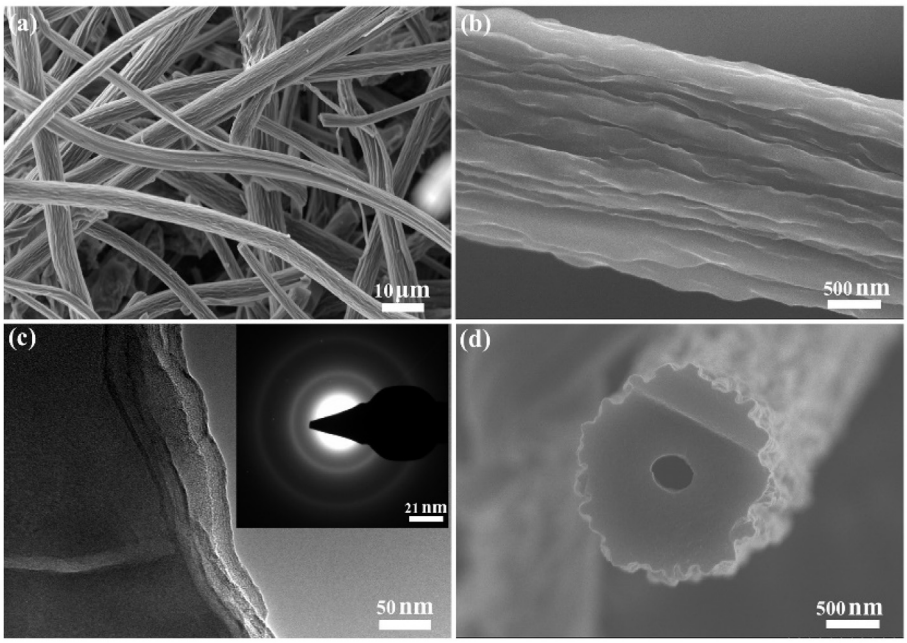

Fig. 2. (a), (b) and (d) SEM images of Carbon fibers evolved from bamboo chopsticks. (c) TEM image of Carbon fibers evolved from bamboo chopsticks (inset: the corresponding SAED pattern).

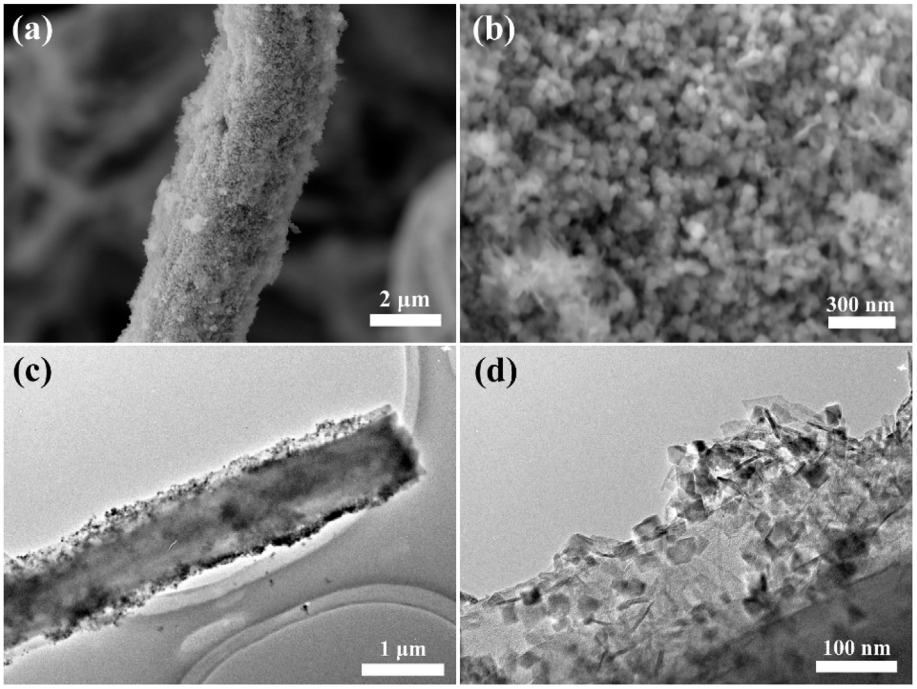

Fig. 3. (a) SEM images and (b) correspondingly enlarged view of CFS/MnO_2. (c) TEM image and (d) correspondingly enlarged view of CFS/MnO_2.

electrodeposition process, the crystal nucleus of MnO_2 is formed first on the surface of CFS derived by the applied voltage of ~1.1 V via the reactions mentioned above and then further grows into nanoparticles. As the thick MnO_2 layer is formed on the carbon fibers for a large mass loading, ~0.6 mg/cm^2, the 3D carbon fiber structure is still maintained without merging into a film. Such a highly porous structure with a large mass loading is excellent for supercapacitors applications.

Judged from the shape of the nitrogen adsorption isotherms shown in Fig. 4(a) and (b), the nitrogen adsorption isotherm of CFS is type IV and that of CFS/MnO_2 is essentially type I mixed with type IV according to the IUPAC classification [38,39]. The CFS/MnO_2 sample presents a higher BET surface area of 68.28 $m^2\ g^{-1}$ than CFS one (only 7.15 $m^2\ g^{-1}$), but the mass ratio of CFS with a low surface area in CFS/MnO_2 reaches up to 87% (4.07/4.67). Therefore, a simple method is introduced to evaluate the surface area of pure MnO_2 nanoparticles due to its firm adhesion on CFS even under a powerful ultrasonic exfoliation. The calculated process is

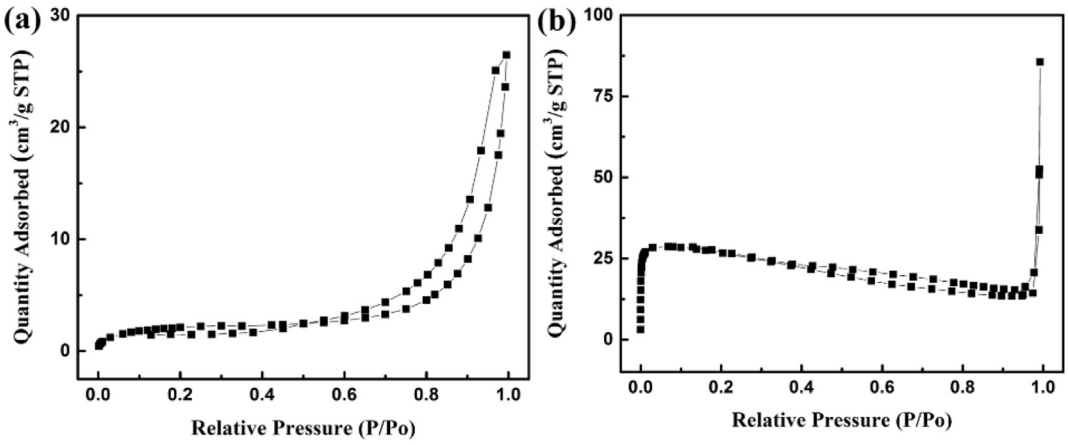

Fig. 4. Nitrogen adsorption–desorption isotherms of (a) the CFS and (b) CFS/MnO_2 samples.

elaborated as follow: The mass density of CFS with the diameter of 2.5 cm fabricated in this work is 4.07 mg cm^{-2} and the mass loading of MnO_2 is confirmed to be 0.6 mg cm^{-2} via the mass variation of CFS before and after electrodeposition. The surface area of CFS is 7.15*X* m^2, where *X* (g) is the CFS mass used in the BET testing. Similarly, the mass of MnO_2 deposited on the CFS is 0.15*X* g (0.6*X*/4.07). Thus, these nanoparticles of MnO_2 provide a large BET specific surface area of 475.18 m^2/g obtained by the formula of (68.28 × 1.15*X*-7.15*X*) m^2/0.15*X* g which is conducive to the diffusion of the electrolyte ions and electrons.

To confirm crystal and local atomic structure of the MnO_2, Raman, XRD and XPS were applied to characterize the resultant CFS/MnO_2 composites. Fig. 5(a) are Raman spectra of CFS and CFS/MnO_2 composites and show two distinct bands located at 1341 cm^{-1} (D band) and 1592 cm^{-1} (G band) corresponding to the breathing mode of k-point phonons of A_{1g} symmetry and the first-order scattering of the E_{2g} phonons in carbon [40]. The relative intensity ratio of D to G bands (I_D/I_G) is usually used to evaluate the degree of graphitization, structural defects and the domain size of graphitic carbon [41]. Compared to the pristine CFS, the I_D/I_G value for CFS/MnO_2 composites increases from 0.96 to 1.04, indicating that the CFS/MnO_2 surfaces mainly existed in the form of amorphous carbon materials [42]. In CFS/MnO_2 composite, a strong absorption band centered around 648 cm^{-1} is ascribed to the Mn-O symmetric stretching vibration of MnO_6 octahedral in MnO_2, suggesting the formation of manganese oxide [43]. The relatively high intensity of the MnO_2 band to C bands suggests a high MnO_2 content in the composites. Fig. 5(b) presents XRD patterns of CFS and CFS/MnO_2 composites. There are two broad diffraction peaks located at about 24.6° and 44.4° for the pattern of CFS, ascribing to the typical (002) and (101) crystal planes of graphitic carbon, respectively [44,45]. It is consistent with the SAED pattern in Fig. 2(c). The XRD pattern of CFS/MnO_2 composites shows two characteristic peaks at 37.1° and 66.1°, albeit very week, indicating the presence of MnO_2 with low crystallinity and/or small quantity. The XPS spectra of CFS and CFS/MnO_2 are presented in Fig. 5(c). C 1s signal, Mn 2p and O 1s peaks are observed. Fig. 5(d) shows the Mn $2p_{3/2}$ and Mn $2p_{1/2}$ peaks located at 642.2 eV and 654.0 eV, respectively, with a spin-energy separation of 11.8 eV, further confirming the presence of MnO_2 in the composite [43].

Fig. 6(a) shows the CV curves of the CFS and CFS/MnO_2 at a scan rate of 100 mV s^{-1}. Compared to CFS electrode, the CV curve of CFS/MnO_2 composite demonstrates a quasi-rectangular shape and no obvious current polarization near the potential of 1 V can be observed. The integral area covered by the CV curve of CFS/MnO_2 composite is much greater than that of CFS, close to 365 times that of CFS, which indicates that CFS is only served as the substrate to provide large specific surface area and good electrical conductivity for the active MnO_2 coating. The CV curves of the CFS/MnO_2 electrodes at different scan rates are demonstrated in Fig. 6(b). The quasi-rectangular CV curves, without obvious Faradic redox peaks, are consistent with an energy storage process. Also, the shape of the CV curves is not significantly affected by the scan rates of CV, revealing a superior electrochemical stability and rate capability of the electrode materials [46]. The GCD curves of CFS/MnO_2 composite electrodes were tested at different charge/discharge currents as presented in Fig. 6(c). The discharge curves are clearly symmetric with its corresponding charge counterparts, and exhibiting a negligible voltage drop (IR_{drop}), indicating a rapid I-V response and an excellent electrochemical reversibility [47,48]. The specific capacitance values (for a single electrode) are estimated to be 375, 290, 247, 213, 145 and 110 F g^{-1} at the current densities of 1, 5, 10, 20, 30 and 50 A g^{-1}. The high specific capacitance is due to simultaneously synergistic effects. That is, the nanoparticles architecture of CFS/MnO_2 can shorten the transport length of ions and enhance the liquid electrolyte transport between the electrode and ions. Meanwhile, the high specific surface area of the active site can provide a convenient and fast electron/ion-transport path [49,50]. Also, the comparative representation of the performances of MnO_2-based supercapacitors reported in other works was presented in Table 1 [14,19,51–56].

Fig. 6(d) presents the calculated specific capacitances of CFS/MnO_2 electrodes at various charge/discharge current density based on these above GCD curves (Fig. 6(c)). The specific capacitance of CFS/MnO_2 at the current density of 1 A g^{-1} reaches to 375 F g^{-1}. Even though the current density increases up to 50 A g^{-1}, the specific capacitance of CFS/MnO_2 still remains 110 F g^{-1}. The inset in Fig. 6(d) shows the specific capacitances of CFS electrodes at various charge/discharge current density. The highest capacitance of CFS electrodes is just 0.42 F g^{-1} at a low current density of 0.1 A g^{-1}, indicating the capacitive performance of CFS/MnO_2 is mainly attribute to MnO_2. However, it is obvious that CFS electrodes provide unbelievable stable rate capability. Hence, CFS/MnO_2 electrodes also demonstrate much excellent rate capability which can be mainly ascribed to reliable electrical connections between the 3D carbon fibers structure and MnO_2. Fig. 6(e) presents the cycling stability of CFS/MnO_2 electrodes at a charge/discharge current density of 20 A g^{-1} for 5000 cycles. After 5000 cycles, 110.3% of the pristine capacitance is retained for CFS/MnO_2 electrodes, signifying super electrochemical stability. It should be noted

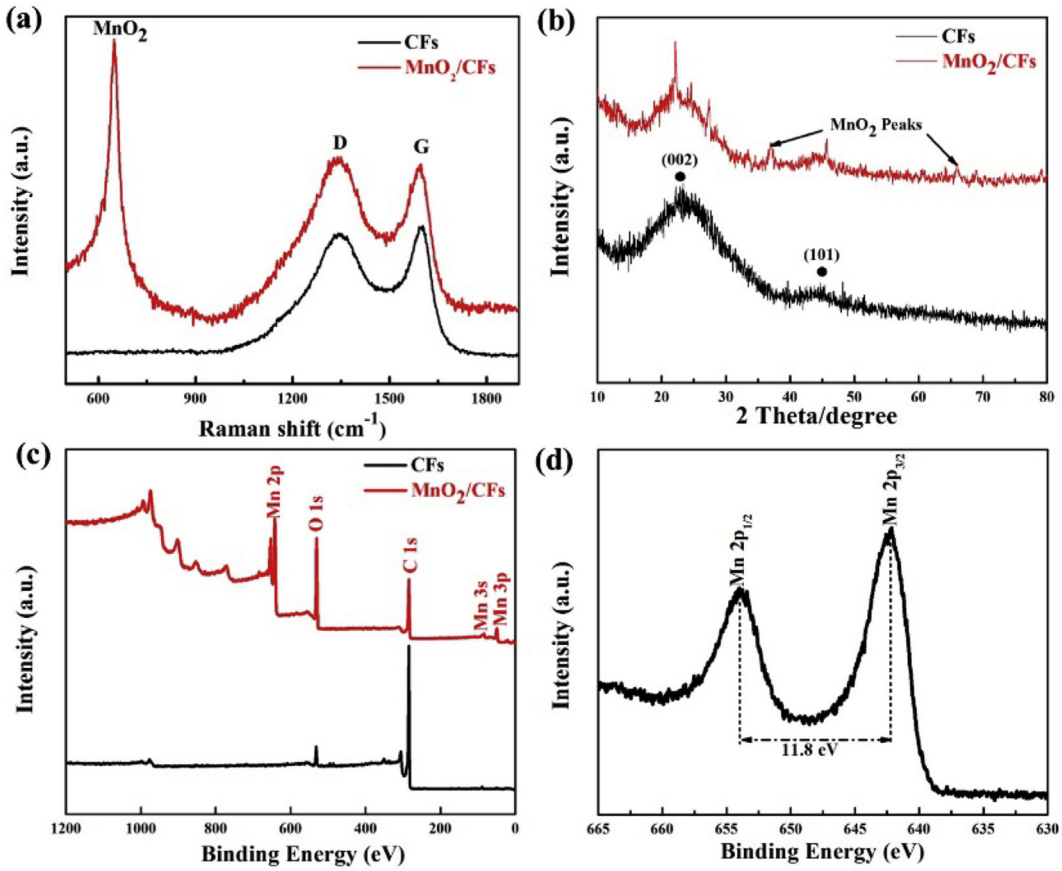

Fig. 5. (a) Raman spectrum, (b) XRD pattern and (c) XPS survey spectra of produced CFS and CFS/MnO_2. (d) XPS spectrum of Mn 2p.

here that the decrease in capacitance retention of CFS/MnO_2 from the initial to the 687th cycle could be due to the mechanical expansion of MnO_2 during the ion insertion/removal process and the dissolution of a little MnO_2 during the charge/discharge cycling [57]. However, the capacitance after 5000 cycles is even increased to 235 F g^{-1} which is more than the initial value, owing to the occurrence of morphological or structural changes of the electrode during the active process. And the increase of the active sites can be attributed to the continuous intercalation-de-intercalation of the ions in the electrode and the low resistance of the current collector (CFS), which can facilitate the effective electron transport in the electrode/electrolyte interface [58,59]. Besides, the EIS curves of the CFS/MnO_2 electrode have been studied in the frequency range from 100 kHz to 1 mHz as shown in Fig. 6(f). At the high frequency region, the starting cross point of a semicircle at Z′ axis indicates a combined resistance (R_c) of ionic for electrolyte, intrinsic resistance of substrate, and contact resistance at the active material/current collector interface [60]. The low R_c of the CFS/MnO_2 electrode slightly decreases from 3.93 Ω to 3.58 Ω after 5000 cycles, confirming the above reasons for the increase of the capacitance after 5000 cycles. Moreover, the CFS/MnO_2 composite electrode after 5000 cycles has a relatively shorter straight line with the slope of 45° which corresponds to the Warburg resistance resulting from faster ion diffusion in the electrolyte and adsorption on the electrode surface [60,61]. At the very low frequency region, the straight line with a large slope demonstrates a good capacitive behavior without diffusion limitation.

To further explore the potential application of our prepared electrodes, a symmetric supercapacitor of CFS/MnO_2//CFS/MnO_2 was tested in 1 M Na_2SO_4 electrolyte. As shown in Fig. 7(a), the CV curves at different scan rates were conducted at a potential window of 0–1 V, showing rectangular-type shapes without obvious redox peaks which indicates good reversibility and ideal capacitive behavior. Fig. 7(b) shows the GCD curves of the symmetric supercapacitor at different charge/discharge current densities ranging from 1 A g^{-1} to 12 A g^{-1}. Quasi linear GCD curves are observed, suggesting a rapid I–V response, small equivalent series resistance and excellent electrochemical reversibility [24]. Based on these GCD curves, the specific capacitances are 79.0, 70.3, 63.9, 54.3, 47.1, 35.0 and 27.9 F g^{-1} at the current densities of 1, 2, 3, 5, 7, 10 and 12 A g^{-1}, respectively, as shown in Fig. 7(c). The EIS data of the symmetric supercapacitor was analyzed by using Nyquist plot over a frequency range of 0.01–10^5 Hz, as shown in Fig. 7(d). It can be observed that the supercapacitor shows relatively low series resistance. Besides, the energy and power density of the symmetric supercapacitor could be calculated in accordance with the specific capacitances. From the Ragone plots in Fig. 7(e), the CFS/MnO_2// CFS/MnO_2 delivers the maximum energy density of 11.0 Wh kg^{-1} at a power density of 529.3 W kg^{-1}, and the maximum power density of 17.4 kW kg^{-1} at an energy density of 3.9 W h kg^{-1}. The long-term cycle stability of the CFS/MnO_2//CFS/MnO_2 examined by using GCD measurements at 6 A g^{-1} for 5000 cycles is shown in Fig. 7(f). A capacitance retention of 99.2% is observed after 5000 cycles, manifesting a good cycling stability. These results further demonstrate that this kind of CFS/MnO_2 nanoparticle structure is very applicable to high performance supercapacitors.

4. Conclusion

A novel type of self-supported binder-free carbon fibers/MnO_2

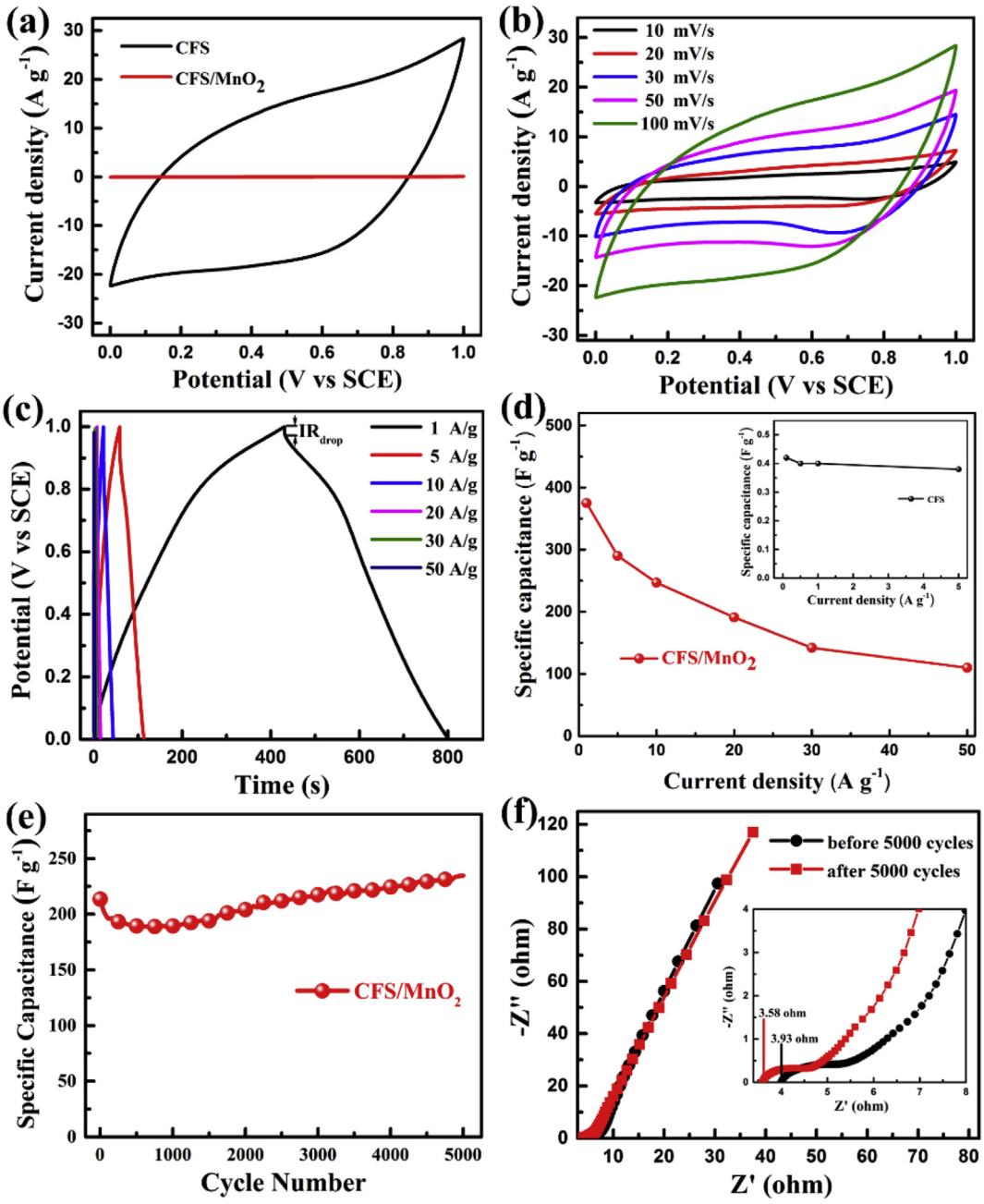

Fig. 6. Electrochemical performances for CFS/MnO_2 electrode. (a) CV curves of CFS and CFS/MnO_2 at a scan rate of 100 mV s^{-1}. (b) CV curves measured in 1 M Na_2SO_4 aqueous solution. (c) Galvanostatic charge/discharge profile. (d) The dependence of specific capacitance of CFS (inset) and CFS/MnO_2 on charge/discharge current density. (e) Charge/discharge cycling test at a current density of 20 A g^{-1}. (f) Nyquist plot of the electrochemical impedance spectra before/after 5000 cycles, respectively. Inset: Magnification of the high frequency region.

Table 1
Comparative representation of the performances of MnO_2-based supercapacitors reported in other similar works.

Electrode materials	The maximum specific capacitance	Retention	Self-supported or binder-free	Reference
3D graphene/carbon nanotubes/MnO_2 nanoneedles	343.1 F g^{-1} at 2 mV s^{-1}	95.3%	Yes	[56]
Graphene/MnO_2 nanoflower	320.59 F g^{-1} at 0.5 A g^{-1}	95.5%	Yes	[52]
MnO_2@PPy	380 F g^{-1} at 1 mV s^{-1}	90%	No	[19]
Mesoporous carbon-carbonaceous materials/MnO_2	326 F g^{-1} at 0.5 A g^{-1}	>100%	No	[14]
Zn_2SnO_4/MnO_2 core/shell nanocable-carbon microfiber	621.6 F g^{-1} at 2 mV s^{-1}	98.8%	Yes	[54]
SWNTs@MnO_2/polypyrrole	351 F g^{-1} at 1 mV s^{-1}	94.4%	Yes	[53]
mesoporous MnO_2/PPy nanofilms	320 F g^{-1} at 0.5 A g^{-1}	91.4%	No	[51]
Graphene/MnO_2	380 F g^{-1} at 0.1 mA cm^{-2}	95%	Yes	[55]
CFS/MnO_2	375 F g^{-1} at 1 A g^{-1}	>100%	Yes	Our work

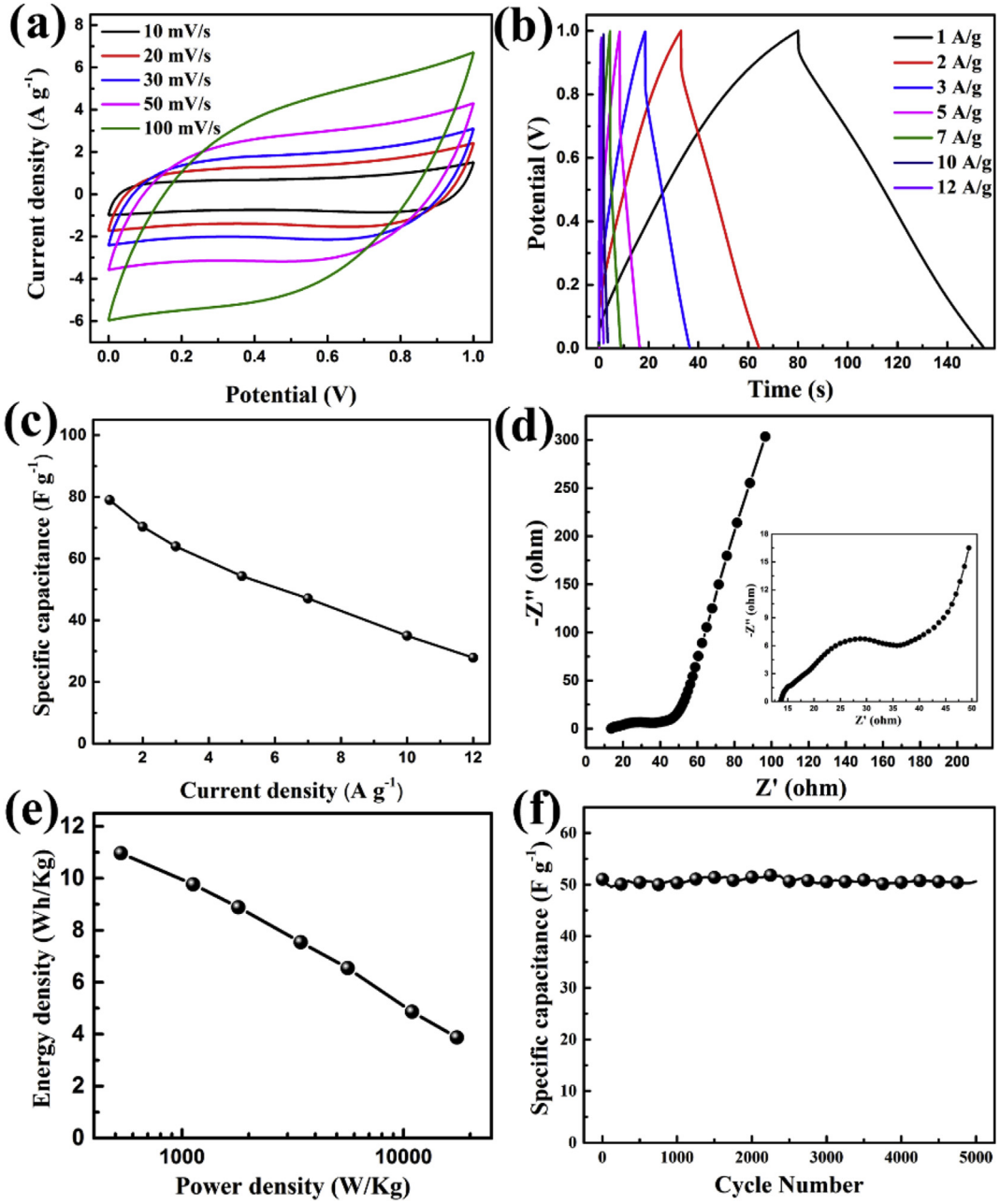

Fig. 7. Electrochemical performances measured in 1 M Na_2SO_4 aqueous solution for the symmetric supercapacitor of CFS/MnO_2//CFS/MnO_2. (a) CV curves at different scan rates. (b) Galvanostatic charge/discharge profile. (c) Specific capacitance at different current densities. (d) Nyquist plot of the electrochemical impedance spectra. Inset: Magnification of the high frequency region. (e) Ragone plots of the symmetric supercapacitor. (f) Charge/discharge cycling test at a current density of 6 A g^{-1}.

composites electrode derived from disposable bamboo chopsticks have been successfully designed and synthesized. The carbon fibers were used as excellent substrate to support high specific surface area for attachment of MnO_2 and provide reliable electrical connection. The resultant MnO_2 on surface of CFS demonstrates nanoparticles with the diameter of 20–50 nm. As a self-supported electrode for supercapacitors, CFS/MnO_2 electrode exhibits much higher specific capacitance of 375 F g^{-1} at current density of 1 A g^{-1}. Moreover, the excellent cycling stability of 110.3% retention is obtained after 5000 cycles. These fascinating electrochemical properties could be due to the fact: 1) the MnO_2 nanoparticles can greatly shorten the diffusion distance of the electrolyte ions during the charge/discharge process, improving the electrochemical utilization of MnO_2; 2) the reliable electrical connections between the particular carbon fibers structure and MnO_2 can facilitate the charge transfer, leading to a high cycle stability. Further, the symmetric supercapacitor comprised of CFS/MnO_2 electrodes presents a maximum energy density of 11 Wh kg^{-1} and a maximum power density of 17.4 kW kg^{-1}. And these impressive results suggest that this well-designed nanostructured carbon fibers/MnO_2 composites in this work might give a new insight into the development of sustainable and environmental friendly energy storage devices.

Acknowledgments

This work was financially supported by National Natural Science Foundation of China (Grant No. 61376011, 51362026).

References

[1] J. Jiang, J. Zhu, W. Ai, Z. Fan, X. Shen, C. Zou, J. Liu, H. Zhang, T. Yu, Evolution of disposable bamboo chopsticks into uniform carbon fibers: a smart strategy to fabricate sustainable anodes for Li-ion batteries, Energy Environ. Sci. 7 (2014) 2670–2679.

[2] J.-G. Wang, F. Kang, B. Wei, Engineering of MnO_2-based nanocomposites for high-performance supercapacitors, Prog. Mater. Sci. 74 (2015) 51–124.

[3] J. Hou, C. Cao, F. Idrees, X. Ma, Hierarchical porous nitrogen-doped carbon nanosheets derived from silk for ultrahigh-capacity battery anodes and supercapacitors, ACS Nano 9 (2015) 2556–2564.

[4] S.L. Candelaria, Y. Shao, W. Zhou, X. Li, J. Xiao, J.-G. Zhang, Y. Wang, J. Liu, J. Li, G. Cao, Nanostructured carbon for energy storage and conversion, Nano Energy 1 (2012) 195–220.

[5] S. Faraji, F.N. Ani, The development supercapacitor from activated carbon by electroless plating—a review, Renew. Sust. Energy Rev. 42 (2015) 823–834.

[6] Z. Yu, L. Tetard, L. Zhai, J. Thomas, Supercapacitor electrode materials: nanostructures from 0 to 3 dimensions, Energy Environ. Sci. 8 (2015) 702–730.

[7] Z. Wang, W. Jia, M. Jiang, C. Chen, Y. Li, Microwave-assisted synthesis of layer-by-layer ultra-large and thin NiAl-LDH/RGO nanocomposites and their excellent performance as electrodes, Sci. China Mater. 58 (2015) 944–952.

[8] W. Li, J. Xu, Y. Pan, L. An, K. Xu, G. Wang, Z. Yu, L. Yu, J. Hu, A facile synthesis of α-MnO_2 used as a supercapacitor electrode material: the influence of the Mn-based precursor solutions on the electrochemical performance, Appl. Surf. Sci. 357 (2015) 1747–1752.

[9] L. Yuan, C. Wan, L. Zhao, Facial in-situ synthesis of MnO_2/PPy composite for supercapacitor, Int. J. Electrochem. Sci. 10 (2015) 9456–9465.

[10] Q. Li, X.F. Lu, H. Xu, Y.X. Tong, G.R. Li, Carbon/MnO_2 double-walled nanotube arrays with fast ion and electron transmission for high-performance supercapacitors, ACS Appl. Mater. Interfaces 6 (2014) 2726–2733.

[11] R. Berenguer, F.J. García-Mateos, R. Ruiz-Rosas, D. Cazorla-Amorós, E. Morallón, J. Rodríguez-Mirasol, T. Corderoa, Biomass-derived binderless fibrous carbon electrodes for ultrafast energy storage, Green Chem. 18 (2016) 1506–1515.

[12] S.L. Candelaria, G. Cao, Increased working voltage of hexamine-coated porous carbon for supercapacitors, Sci. Bull. 60 (2015) 1587–1597.

[13] S.L. Candelaria, E. Uchaker, G. Cao, Comparison of surface and bulk nitrogen modification in highly porous carbon for enhanced supercapacitors, Sci. China Mater. 58 (2015) 521–533.

[14] Z. Wen, M. Li, S. Zhu, T. Wang, Novel mesoporous carbon-carbonaceous materials nanostructures decorated with MnO_2 nanosheets for supercapacitors, Int. J. Electrochem. Sci. 11 (2016) 1810–1820.

[15] C. Ramirez-Castro, O. Crosnier, L. Athouel, R. Retoux, D. Belanger, T. Brousse, Electrochemical performance of carbon/MnO_2 nanocomposites prepared via molecular bridging as supercapacitor electrode materials, J. Electrochem. Soc. 162 (2015) A5179–A5184.

[16] Y. Zhao, W. Ran, J. He, Y. Huang, Z. Liu, W. Liu, Y. Tang, L. Zhang, D. Gao, F. Gao, High-performance asymmetric supercapacitors based on multilayer MnO_2/graphene oxide nanoflakes and hierarchical porous carbon with enhanced cycling stability, Small 11 (2015) 1310–1319.

[17] J. Yan, Z. Fan, T. Wei, W. Qian, M. Zhang, F. Wei, Fast and reversible surface redox reaction of graphene–MnO_2 composites as supercapacitor electrodes, Carbon 48 (2010) 3825–3833.

[18] J. Liu, J. Essner, J. Li, Hybrid supercapacitor based on coaxially coated manganese oxide on vertically aligned carbon nanofiber arrays, Chem. Mater. 22 (2010) 5022–5030.

[19] W. Yao, H. Zhou, Y. Lu, Synthesis and property of novel MnO_2@polypyrrole coaxial nanotubes as electrode material for supercapacitors, J. Power Sources 241 (2013) 359–366.

[20] S. He, W. Chen, 3D graphene nanomaterials for binder-free supercapacitors: scientific design for enhanced performance, Nanoscale 7 (2015) 6957–6990.

[21] Y. Zou, S. Wang, Interconnecting carbon fibers with thein-situ electrochemically exfoliated graphene as advanced binder-free electrode materials for flexible supercapacitor, Sci. Rep. 5 (2015) 11792.

[22] W. Zuo, C. Wang, Y. Li, J. Liu, Directly grown nanostructured electrodes for high volumetric energy density binder-free hybrid supercapacitors: a case study of CNTs//$Li_4Ti_5O_{12}$, Sci. Rep. 5 (2015).

[23] Y. Fang, J. Liu, D.J. Yu, J.P. Wicksted, K. Kalkan, C.O. Topal, B.N. Flanders, J. Wu, J. Li, Self-supported supercapacitor membranes: polypyrrole-coated carbon nanotube networks enabled by pulsed electrodeposition, J. Power Sources 195 (2010) 674–679.

[24] T. Qin, B. Liu, Y. Wen, Z. Wang, X. Jiang, Z. Wan, S. Peng, G. Cao, D. He, Free-standing flexible graphene foams@polypyrrole@MnO_2 electrodes for high-performance supercapacitors, J. Mater. Chem. A 4 (2016) 9196–9203.

[25] R. K., S. Jain, U.C. Jindal, Mechanical behaviour of bamboo and bamboo composite, J. Mater. Sci. 27 (1992) 4598–4604.

[26] H.P.S. Abdul Khalil, I.U.H. Bhat, M. Jawaid, A. Zaidon, D. Hermawan, Y.S. Hadi, Bamboo fibre reinforced biocomposites: a review, Mater. Des. 42 (2012) 353–368.

[27] Z. Gui, H. Zhu, E. Gillette, X. Han, G.W. Rubloff, L. Hu, S.B. Lee, Natural cellulose fiber as substrate for supercapacitor, ACS Nano 7 (2013) 6037–6046.

[28] D. Puthusseri, V. Aravindan, B. Anothumakkool, S. Kurungot, S. Madhavi, S. Ogale, From waste paper basket to solid state and Li-HEC ultracapacitor electrodes: a value added journey for shredded office paper, Small 10 (2014) 4395–4402.

[29] P. Xu, B. Wei, Z. Cao, J. Zheng, K. Gong, F. Li, J. Yu, Q. Li, W. Lu, J.-H. Byun, B.-S. Kim, Y. Yan, T.-W. Chou, Stretchable wire-shaped asymmetric supercapacitors based on pristine and MnO_2 coated carbon nanotube fibers, ACS Nano 9 (2015) 6088–6096.

[30] Z. Zhang, F. Xiao, S. Wang, Hierarchically structured MnO_2/graphene/carbon fiber and porous graphene hydrogel wrapped copper wire for fiber-based flexible all-solid-state asymmetric supercapacitors, J. Mater. Chem. A 3 (2015) 11215–11223.

[31] M.D. Stoller, R.S. Ruoff, Best practice methods for determining an electrode material's performance for ultracapacitors, Energy Environ. Sci. 3 (2010) 1294.

[32] J. Jiang, J. Liu, R. Ding, J. Zhu, Y. Li, A. Hu, X. Li, X. Huang, Large-scale uniform alpha-$Co(OH)_2$ long nanowire arrays grown on graphite as pseudocapacitor electrodes, ACS Appl. Mater. Interfaces 3 (2011) 99–103.

[33] B. Aleman, M.M. Bernal, B. Mas, E.M. Perez, V. Reguero, G. Xu, Y. Cui, J.J. Vilatela, Inherent predominance of high chiral angle metallic carbon nanotubes in continuous fibers grown from a molten catalyst, Nanoscale 8 (2016) 4236–4244.

[34] S.C. Narayanan, K.R. Karpagam, A. Bhattacharyya, Nanocomposite coatings on cotton and silk fibers for enhanced electrical conductivity, Fiber. Polym. 16 (2015) 1269–1275.

[35] H. Wang, C. Ma, X. Yang, T. Han, Z. Tao, Y. Song, Z. Liu, Q. Guo, L. Liu, Fabrication of boron-doped carbon fibers by the decomposition of B_4C and its excellent rate performance as an anode material for lithium-ion batteries, Solid State Sci. 41 (2015) 36–42.

[36] Y. Zhu, S. Murali, M.D. Stoller, K.J. Ganesh, W. Cai, P.J. Ferreira, A. Pirkle, R.M. Wallace, K.A. Cychosz, M. Thommes, D. Su, E.A. Stach, R.S. R., Carbon-based supercapacitors produced by activation of graphene, Science 332 (2011) 1537–1541.

[37] S. Rodrigues, A. Shukla, N. Munichandraiah, A cyclic voltammetric study of the kinetics and mechanism of electrodeposition of manganese dioxide, J. Appl. Electrochem. 28 (1998) 1235–1241.

[38] A. Vinu, D.P. Sawant, K. Ariga, M. Hartmann, S.B. Halligudi, Benzylation of benzene and other aromatics by benzyl chloride over mesoporous AlSBA-15 catalysts, Microporous Mesoporous Mater. 80 (2005) 195–203.

[39] K.S.W. Sing, D.H. Everett, R.A.W. Haul, L. Moscou, R.A. Pierotti, J. Rouquerol, T. Siemieniewska, Reporting physisorption data for gas-solid systems with special reference to the determination of surface area and porosity, Pure Appl. Chem. 57 (1985) 603–619.

[40] S.H. Aboutalebi, A.T. Chidembo, M. Salari, K. Konstantinov, D. Wexler, H.K. Liu, S.X. Dou, Comparison of GO, GO/MWCNTs composite and MWCNTs as potential electrode materials for supercapacitors, Energy Environ. Sci. 4 (2011) 1855.

[41] W. Gao, Y. Wan, Y. Dou, D. Zhao, Synthesis of partially graphitic ordered mesoporous carbons with high surface areas, Adv. Energy Mater. 1 (2011) 115–123.

[42] D. Shao, J. Li, X. Wang, Poly(amidoxime)-reduced graphene oxide composites as adsorbents for the enrichment of uranium from seawater, Sci. China Chem. 57 (2014) 1449–1458.

[43] D. Zhou, H. Lin, F. Zhang, H. Niu, L. Cui, Q. Wang, F. Qu, Freestanding MnO_2 nanoflakes/porous carbon nanofibers for high-performance flexible supercapacitor electrodes, Electrochim. Acta 161 (2015) 427–435.

[44] S. Hwang, S. Lee, J.-S. Yu, Template-directed synthesis of highly ordered nanoporous graphitic carbon nitride through polymerization of cyanamide, Appl. Surf. Sci. 253 (2007) 5656–5659.

[45] Q. Wang, J. Yan, Y. Xiao, T. Wei, Z. Fan, M. Zhang, X. Jing, Interconnected porous and nitrogen-doped carbon network for supercapacitors with high rate capability and energy density, Electrochim. Acta 114 (2013) 165–172.

[46] M. Ramezani, M. Fathi, F. Mahboubi, Facile synthesis of ternary MnO_2/graphene nanosheets/carbon nanotubes composites with high rate capability for supercapacitor applications, Electrochim. Acta 174 (2015) 345–355.

[47] L. Chang, W. Wei, K. Sun, Y.H. Hu, 3D flower-structured graphene from CO_2 for supercapacitors with ultrahigh areal capacitance at high current density, J. Mater. Chem. A 3 (2015) 10183–10187.

[48] H.Y. Jung, M.B. Karimi, M.G. Hahm, P.M. Ajayan, Y.J. Jung, Transparent, flexible supercapacitors from nano-engineered carbon films, Sci. Rep. 2 (2012) 773.

[49] Y. Jin, H. Chen, M. Chen, N. Liu, Q. Li, Graphene-patched CNT/MnO_2 nanocomposite papers for the electrode of high-performance flexible asymmetric supercapacitors, ACS Appl. Mater. Interfaces 5 (2013) 3408–3416.

[50] Y.S. Yun, S.Y. Cho, J. Shim, B.H. Kim, S.J. Chang, S.J. Baek, Y.S. Huh, Y. Tak, Y.W. Park, S. Park, H.J. Jin, Microporous carbon nanoplates from regenerated silk proteins for supercapacitors, Adv. Mater. 25 (2013) 1993–1998.

[51] N. Wang, P. Zhao, K. Liang, M. Yao, Y. Yang, W. Hu, CVD-grown polypyrrole nanofilms on highly mesoporous structure MnO_2 for high performance asymmetric supercapacitors, Chem. Eng. J. 307 (2017) 105–112.

[52] Y. Zheng, W. Pann, D. Zhengn, C. Sun, Fabrication of functionalized graphene-based MnO_2 nanoflower through electrodeposition for high-performance supercapacitor electrodes, J. Electrochem. Soc. 163 (2016) D230–D238.

[53] K. Liang, T. Gu, Z. Cao, X. Tang, W. Hu, B. Wei, In situ synthesis of SWNTs@MnO_2/polypyrrole hybrid film as binder-free supercapacitor electrode, Nano Energy 9 (2014) 245–251.

[54] L. Bao, J. Zang, X. Li, Flexible Zn_2SnO_4/MnO_2 core/shell nanocable-carbon microfiber hybrid composites for high-performance supercapacitor electrodes, Nano Lett. 11 (2011) 1215–1220.

[55] G. Yu, L. Hu, N. Liu, H. Wang, M. Vosgueritchian, Y. Yang, Y. Cui, Z. Bao,

Enhancing the supercapacitor performance of graphene/MnO_2 nanostructured electrodes by conductive wrapping, Nano Lett. 11 (2011) 4438–4442.
[56] M. Kim, Y. Hwang, J. Kim, Fabrication of graphene-carbon nanotube papers decorated with manganese oxide nanoneedles on the graphene sheets for supercapacitors, Phys. Chem. Chem. Phys. 16 (2014) 351–361.
[57] Y. He, W. Chen, X. Li, Z. Zhang, J. Fu, C. Zhao, E. Xie, Freestanding three-dimensional graphene/MnO_2 composite networks as ultralight and flexible supercapacitor electrodes, ACS Nano 7 (2013) 174–182.
[58] S. Nagamuthu, S. Vijayakumar, G. Muralidharan, Synthesis of Mn_3O_4/amorphous carbon nanoparticles as electrode material for high performance supercapacitor applications, Energy Fuel 27 (2013) 3508–3515.
[59] K.V. Sankar, D. Kalpana, R.K. Selvan, Electrochemical properties of microwave-assisted reflux-synthesized Mn_3O_4 nanoparticles in different electrolytes for supercapacitor applications, J. Appl. Electrochem. 42 (2012) 463–470.
[60] Z. Fan, J. Yan, T. Wei, L. Zhi, G. Ning, T. Li, F. Wei, Asymmetric supercapacitors based on graphene/MnO_2 and activated carbon nanofiber electrodes with high power and energy density, Adv. Funct. Mater. 21 (2011) 2366–2375.
[61] M. Kim, I. Oh, J. Kim, Supercapacitive behavior depending on the mesopore size of three-dimensional micro-, meso- and macroporous silicon carbide for supercapacitors, Phys. Chem. Chem. Phys. 17 (2015) 4424–4433.